Extended Abstracts of the 16th (1984 International) Conference on Solid State Devices and Materials, Kobe, 1984

Invited **B-4-1**

RECENT ADVANCES AND APPLICATIONS OF SIMS TO ELECTRONIC MATERIALS

Charles A. Evans, Jr.
Charles Evans & Associates
1670 S. Amphlett Blvd., Suite 120
San Mateo, California 94402
(415) 572- 1601

The energetic ion bombardment of a material causes the outermost layers to be ejected by sputtering. A small fraction of the sputtered species are ejected as positive or negative ions and can be analyzed by a mass spectrometer to provide a sensitive qualitative and quantitative microanalysis of the bombarded material. The ion probe/SIMS can provide lateral microanalysis with sub-micron resolution or in-depth profiles with sub-ppm detection limits. If each depth-profiling data point is taken from an area of 150 micrometers in diameter and a depth of 100 Angstroms, sensitivities will range from 10^{12} to 10^{14} atoms/cm^3 for certain dopant elements (ex. B, Li, Na, K, Al, Sb, Cr, Se, Te) to 10^{16} atoms/cm^3 for other dopants and impurities. This discussion will briefly outline the ion production process and instrumentation and describe several application studies.

An increasing interest in the analysis of surfaces and the need for three-dimensional characterization of materials has led to the development of secondary ion mass analysis or ion microprobe mass spectrometry. The "ion probing" of a material is accomplished by bombarding the sample to be analyzed with a beam of 1 to 20 keV ions. These primary ions cause the upper atomic layers to be "sputtered" or stripped off. Most of the material leaves as neutral atoms or molecules, but a small fraction is ejected as positive or negative ions. These secondary ions are then extracted into a mass spectrometer for mass/charge separation to provide an analysis of that portion of the material sampled by the primary ion beam. The mass spectrometer provides elemental coverage from hydrogen to uranium, isotopic characterization, and detection sensitivities for as little as 10^{-15} to 10^{-19} gram, depending on the element under consideration. Since the analytical sample volume at any moment is bounded by the primary beam periphery and extends to a depth of 5 to 50 Angstroms, the operating mode of the instrument can be selected to provide several types of analysis. In-depth analysis is provided by the advancement of the analytical volume through continuous exposure of new material by the sputtering process. Complete mass spectra can be obtained every 25 to 2500 Angstroms, depending on instrumental operating conditions, to provide a characterization of the outer atomic layers of the sample. Alternately, the repetitive monitoring of one or more masses versus time will give isotopic and concentration variations as a function of depth, the so-called depth profile. Localization of the secondary ion production can provide lateral (x,y) chemical analysis with resolutions of 1 micrometer using secondary ion images.

ION PRODUCTION

The detailed processes involved in the production of secondary ions are quite complex and the lack of understanding about these processes has been a major hurdle in the use of SIMS for materials analysis. However, recent studies of secondary ion production have shown the overall process to be rather easy to understand. The primary ions

penetrate to a mean depth in the bombarded material and become incorporated in the outer layers of the sample. During penetration they transfer energy to the matrix atoms, causing lattice bonds to be broken and some atomically bound electrons to be ejected into the conduction band of the material. Positive and negative secondary ions are continually being produced and their detection depends on the mass spectrometer settings at any given time.

Thus, in either case, the ionization phenomena can be thought of in terms of an electron exchange process between the departing atom and the bombarded surface. Positive ionization requires that the atom give up an electron and the surface (or the vacuum) accept it. Conversely, negative ion formation requires that the surface eject an electron and the atom accept one. In the case of a pure metal and inert gas ion bombardment, any positive ion formed in or near the solid is rapidly neutralized by conduction band electrons and is, therefore, not available for detection. Some negative species will be produced by acceptance of these electrons by departing neutral atoms to produce negative secondaries. In neither case, however, are the ion intensities very large. This is the so-called "kinetic" ionization proces since ionization comes about from the kinetic energy exchanged during the sputtering process.

It has been known for years that the presence of oxygen or other reactive species (such as fluorine) greatly enhances the production of positive secondary ions while cesium will increase the yield of negative secondary ions.* Therefore, it is common to introduce oxygen into the near surface region of the sample either by maintaining a high partial pressure of oxygen (1×10^{-5} Torr) in the sample chamber or by using oxygen primary ion beam for sputtering. In this manner, greater analytical sensitivity is obtained and a more quantitative analysis can be performed since minor variations in the sample chemistry do not have as strong an effect on the ion yields as they would. Several workers are now using Cs^+ primary ion beams to provide an enhancement of the negative secondary ions.

The relative yields of the different elements contained within a single matrix and the change in ion yield of a given element when going from one matrix to another can be explained in terms of the electron exchange concept. For the elements contained within a single matrix, the governing factor is the ease with which an atom will give up an electron (to produce a positive ion) or take in an electron (to produce a negative ion). The electron availability is the same to all of the ejected species since they are all coming from the same matrix. The quantitative measure of the relative ion yields is given by an exponential dependence on the inverse of the ionization potential for positive ion formation and the electron affinity for negative ion formation. That is:

$$n^+/n^o \simeq e^{-IP/Y^+} \quad \text{and} \quad n^-/n^o \simeq e^{EA/Y^-} \qquad (1)$$

where Y^+ and Y^- are variables which determine the slope of the relationship. Thus, those elements with a low ionization potential are more sensitive by positive ion spectroscopy while those with a high electron affinity are best analyzed by negative ion spectroscopy. Thus, within a given matrix, the various atomic ion intensities can be evaluated using the above relationships.

Should one examine a given element in several different matrices, the role of the matrix in the electron exchange process must be examined. The degree of acceptance of the matrix for an electron (to produce a positive secondary ion) is governed by a power function dependence on the amount of oxygen (or other reactive species) in the near-surface region of the sample. Conversely, the relative availability of electrons for the electron attachment process is measured by a power function dependence on the cesium (or cesium-like

*The sputtering yield is defined as the number of atoms removed per primary ion while the ion yield is the number of ions produced per ejected atom of that particular element.

elements) near-surface concentration. In the case of a material which does not naturally contain oxygen or cesium, the near-surface concentration is proportional to the inverse of the matrix sputtering yield for oxygen or cesium ion bombardment. Thus, the variation in ion yield and hence the variation in analytical sensitivity of an element from one matrix to another can be explained by:

$$n^+/n^o \propto [O]^{x+} \propto [1/S]^{x+} \quad (2)$$

$$n^-/n^o \propto [Cs]^{x-} \propto [1/S]^{x-} \quad (3)$$

This matrix dependent variation in secondary ion yield is sometimes called a matrix effect and is seen to be due to not the matrix atoms themselves but how the matrix influences the concentration of the incorporated oxygen or cesium.

It is important to emphasize that the detection of a SIMS analytical signal depends on the removal of atoms from the sample and the detection limits depend on:

1. The volume of material and hence, the number of host/matrix atoms removed for each data point;

2. The concentration of the element or elements of interest;

3. The probability that a given atom of interest will be ionized upon sputtering ("the secondary ion yield");

4. The percentage of the secondary ions emitted from that will reach the detector (the spectrometer extraction efficiency and transmission).

Since ion yields can be of the order of 10^{-4} to 10^{-1} and transmissions of the more sophisticated ion probes can be 5% to 10%, an analytical volume 150 micrometers in diameter and 100 Angstroms deep will permit 10^{14} atoms/cm^3 detection limits for elements such as B, In, Cr, Mn, As and the alkali metals. The detection of contaminants such as H, C, O and N is influenced by the quality of the instrument residual vacuum with 10^{15} to 10^{16} atoms/cm^3 attainable if ultra-high vacuum conditions are available.

INSTRUMENTATION

There are a wide variety of instrumental configurations used for secondary ion mass spectrometry. These range from the quadrupole mass filters used in conjunction with other surface analytical techniques to the dedicated ion microanalyzers. Thus, the applications for these different types of SIMS instruments will differ based on the instrumental configuration. The attainment of large dynamic range with high sensitivity requires very specialized instrumentation. These include a high brightness source of oxygen and cesium ions, ion beam focusing optics, an ultra high vacuum sample chamber with a versatile sample stage, an efficient secondary ion extraction and spectrometry system and a low noise, high gain detector. Only if these capabilities are properly implemented, can one expect to attain the full capabilities of the secondary ion mass spectrometry technique.

APPLICATION STUDIES

I. Depth Profiling Detection Limits of $7x10^{14}$ atoms/cm^3 for As in Si.

Silicon wafer samples were used to demonstrate the performance of the cesium source ion microprobe. The wafers were ion implanted with As at an energy of 200 keV to fluences (Φ) of $5x10^{14}$ and $1x10^{12}$ atom/cm^2, respectively. Peak arsenic concentrations $[As]_p$ corresponding to these fluences were calculated according to the formula:

$$[As]_p \simeq 0.4\,\Phi/\Delta R_p \quad (4)$$

Where ΔR_p is the calculated standard deviation of the projected range, obtained from published tables. The respective peak concentrations were

calculated to be $5x10^{19}$ and $1x10^{17}$ atom/cm^3.

Depth profiles were obtained by rastering the primary Cs^+ beam over an area 250 micrometers square to erode a square flat-bottomed crater. The 70 nA Cs^+ beam was focused to a diameter of 30 micrometers at the sample. An electronic aperturing technique was used to ensure that mass-analyzed secondary ions sputtered from the sample were counted only when the primary ion beam was situated within an area 80 micrometers square at the center of the crater. Signal contributions from the crater walls were thereby largely eliminated.

Depth profiles of the two As implant samples are shown in Figure 1. In recording these profiles the $^{75}As^{28}Si^-$ species was monitored rather than $^{75}As^-$. We have noted that the secondary ion yield of low electron affinity species such as As (EA_{As} = 0.8 eV) is higher for diatomic ions incorporating a matrix atom if the matrix species has a higher electron affinity (EA_{Si} = 1.4 eV). In this case, the yield improvement was by a factor of about 3. No difference in shape was seen between profiles of the same sample obtained using the As^- and $AsSi^-$ species.

The high dose profile deviates from a Gaussian shape at $5x10^{17}$ atom/cm^3, and approaches a constant level equivalent to $5x10^{16}$ atom/cm^3. It is known that As ion implants frequently show exponential tails apparently due to diffusion, and they may also exhibit channeling effects. However, since the true profile of this sample is not known, for purposes of this paper we pessimistically ascribe the tailing to an instrumental limitation, namely, inability of the electronic aperturing technique to completely discriminate against $AsSi^-$ ions sputtered from the high As region exposed in the crater wall. That $5x10^{16}$ atom/cm^3 is not a true background level is shown in the profile of the low dose implant which does not show appreciable background tailing above $1x10^{16}$ atom/cm^3.

The low dose profile exhibits an exponential tail which is much more marked than that of the high dose sample in agreement with previous work. The

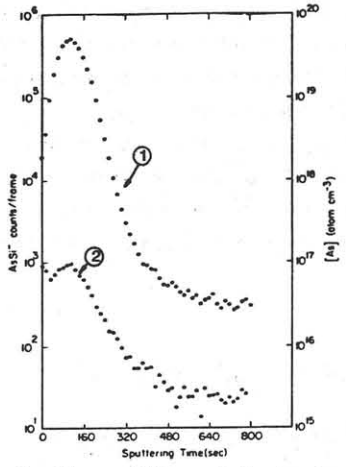

FIGURE 1. Depth profiles of As implants in Si. (1) $5x10^{14}$ As atoms/cm^2, 200 keV; (2) $1x10^{12}$ As atoms/cm^2), 200 keV. Primary species, Cs^+. Analytical species, $AsSi^-$. No background subtraction.

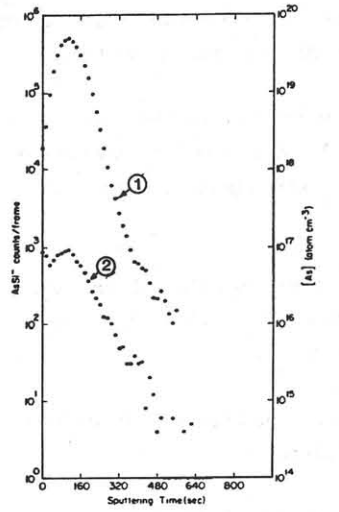

FIGURE 2. Depth profiles of As implants in Si. (1) $5x10^{14}$ As atoms/cm^2, 200 keV; (2) $1x10^{12}$ As atoms/cm^2, 200 keV. Primary species, Cs^+. Analytical species, $AsSi^-$. Background subtracted.

profile approaches a constant background level equivalent to 2 - $3x10^{15}$ atom/cm^3. This level, corresponding to an average count rate of 24 ions/frame, we believe is a true background level because it is apprciably higher (2% of peak concentration) than the aperture limit exhibited by the high dose profile (0.1% of peak concentration). Both profiles were taken under identical conditions. Subtraction of the

instrumental background from the high dose profile and of the true background from the low dose profile yields the corrected profiles shown in Figure 2.

The above is abstracted from Applied Physics Letters 30, 560 (1977).

II. Anomalous Migration of Fluorine and the Electrical Activation of Boron in BF_2^+ Implanted Silicon

Fluorine distribution profiles for silicon implanted with 150 keV $1x10^{15}$ cm^{-2} BF_2^+ at room temperature or at -110°C have been measured by SIMS as a function of anneal temperature. Anomalous migration of fluorine during annealing is observed, and is explained in terms of recrystallization and impurity gettering effects. Electrical carrier distribution profiles of room temperature BF_2^+ implanted silicon, measured by differential Hall effects methods, demonstrate

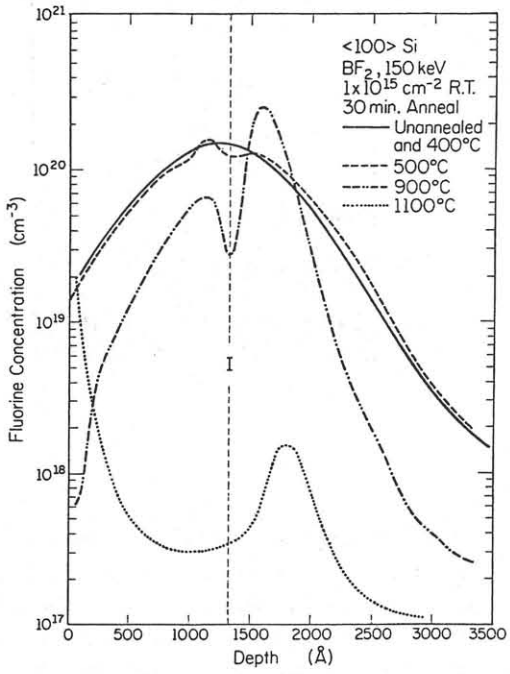

FIGURE 3. Fluorine profiles obtained from SIMS measurements on ◊00◊ Si implanted at room temperature with a $1x10^{15}$ cm^{-2} fluence of BF_2^+ and annealed for 30 min at the temperatures shown. A thin dashed line (I) represents the amorphous-crystalline interface after implantation.

that boron is electrically activated by epitaxial recrystallization during 550°C annealing. However, a damaged region near the cyrstalline-amorphous interface remains after recrystallization. This damaged layer is apparently responsible for the fluorine gettering. This anomolous migration and decoration of the residual damage is shown in the SIMS profiles of Figure 3. This gettering of fluorine by defects was then used as a sensitive marker of the extent of lattice reordering under a variety of implantation and annealing conditions.

More complete reports of these studies have been reported in Applied Physics Letters 32, 144 (1978) and "Recrystallization of Implanted Amorphous Silicon Layers: II. Migration of Fluorine in BF_2^+-Implanted Silicon" by M. Y. Tsai, D. S. Day, B. G. Streetman, P. Williams and C. A. Evans, Jr., published in the Journal of Applied Physics.

III. Direct Lateral and In-Depth Distributional Analysis for Ionic Contaminants in Semiconductor Devices

It is widely known in the semiconductor industry that incorporation of the ionic contaminants Li, Na, K can cause severe reduction of device performance and can result in the loss of production yields. These species are generally detected indirectly by the actual failure of the device under temperature and voltage stress. The recent availability of sensitive ion microanalyzer/SIMS instrumentation allows the direct determination of the ionic species and its location. Thus, it becomes easier to identify the production step which is introducing these ion contaminants. The very mechanism which makes these species deterimental to semiconductor devices, i.e., their low ionization potential, makes them extremely sensitive by the SIMS technique. Therefore, since we detect one ion count of Li, Na, or K for every 10^2 to 10^3 ions sputtered from the sample, detection limits of the order of 10^{12} to 10^{13} atoms/cm^3 can be obtained.

Ionic contaminants can be incorporated from two basic sources. The first is general environmental

contamination (dust and dirt) from the production environment. The second is the introduction of the ionic species during a production process, either from the materials being used or contamination from a piece of processing equipment. By examining the relative concentrations of the ionic contaminants and interelement correlations, one can begin to identify the nature of the incorporation process. If the species are found in accordance with their abundance in dust and dirt, known as the crustal abundance, one then suspects that the origin of the contaminant is environmental material. Alternatively, if one or more of the elements is contained in different proportions than would be expected for an environmental contaminant, then a particular processing step may have actually introduced it as a specific contaminant rather than as a general contaminant.

Additional information on the nature and source of the contamination can be obtained by examining lateral distributional images of the contamination. Therefore, if one detects Na, K or Li in discreet areas as would be produced by particulate contamination, then environmental contamination is indicated. Alternatively, if the suspected ionic contaminants are contained homogeneously within a given feature, one then assumes that the contamination was introduced by the process itself, such as being co-sputtered onto the samples or co-deposited from an evaporation. Therefore, a large body of information on the nature of an ionic contamination can be generated from the three-dimensional distribution of these detrimental trace elements.

The sensitivity of the SIMS technique to the ionic contaminants, Li, Na and K, and the relative abundances of these species as found in nature, can be illustrated by examination of the surface of a virgin silicon wafer. Figure 4 shows the intensity of Li, Na and K versus time while sputtering the surface of a clean silicon wafer. The first region shows the relative intensities for these ionic species from a well-sputtered silicon surface. This establishes the background intensities for the Na, Li and K. If one rapidly translates the sample underneath the beam to an unsputtered region of the surface, we see a sudden increase in the intensity of these three alkalai elements. Note that this logarithmic curve shows over 1×10^5 counts per second of Na and K and approximately 300 counts per second of Li from a supposedly clean surface. As we sputter through the contaminated surface and back into the bulk, the equilibrium background levels of Li, Na and K are reproduced. These count rate differences illustrate the SIMS sensitivity for these species

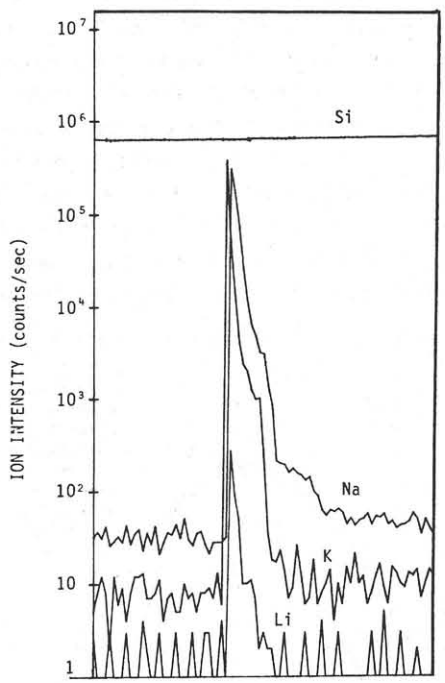

FIGURE 4. Relative ion intensity (counts/second) for the ionic contaminants Li, Na and K on a virgin silicon wafer. The initial low levels for the impurities (less than 100 counts/second) correspond to the equilibrium background. The impurity spikes result from a translation of the speciment to an unsputtered "clean" surface region where the signals increase abruptly. After sputtering away the surface contamination, the impurity signal intensities can be seen to decrease to the bulk background levels.

as well as their relative abundances from natural environmental contamination.

We have used this technique to examine the in-depth distribution of these ionic contaminants in thin films of silicon dioxide, plasma silicon nitrides, evaporated layers of gold and aluminum and sputtered layers of titanium-tungsten alloy. Each of these types of materials is shown to have a differing composition of ionic species as well as in-depth distributions. An example is seen when sputtering an evaporated layer of gold on titanium-tungsten alloy on a silicon wafer substrate. In this case, the ionic contaminants Na and K are relatively low in the evaporated layer, whereas Li is quite high, suggesting that Li has been selectively introduced during the evaporation. However, Li is lower in the sputtered layer than in the gold but Na and K are higher than in the gold. More importantly, K and Na are contained rather homogeneously throughout the titanium-tungsten layer. We attribute the relatively high level of contamination in the Ti-W layer to the incorporation of environmental contaminants, dust and dirt, during the preparation of the powder which is subsequently hot pressed to form the sputtering target and results in the direct co-deposition of the ionic contaminants.

We then examined a failed device for the relative in-depth distribution of the ionic contaminants. For such an analysis we generally collect the ions from a large area of the device (100 to 150 microns in diameter) in order to determine the effects of the different processing steps and hence examine the total amount of ionic contamination contained within the device. Even though the species are only detrimental when contained in a critical location, it may be that the stressing of time and temperature has yet to deliver these species to the sensitive areas and therefore the probability of failure is best measured by examining the total ionic contamination of the device rather than that specifically located inside the gate oxide.

Figure 5 shows the depth profile for Na, K and Li starting at the SiO_2/Si interface in a fully processed working device. The high Na and K concentration observed at the SiO_2/Si interface is chracteristic of the gettering of the ionic species to this region. As the profile goes deeper into the material, the Na and K drop off but we see the Li actually comes up to a level higher than is observed at the passivation-device interface. The modulation in intensity of Na and K results from their being incorporated during different processing steps and hence appearing at different depths in the profile. Alternatively, Li, the most mobile of the ionic species, is seen to actually peak inside the material at the second and third shoulders of the Na and K. All three elements then fall to background levels deeper into the device. Due to the sputtering rate differences of the materials within the analytical area, the sputtering front progresses through the device unevenly. Hence, the interfaces between different layers representing metallizations, etc., are not as discreet as would be obtained in a normal thin film profile. Figure 6 shows the profile of a similar device as in Figure 5

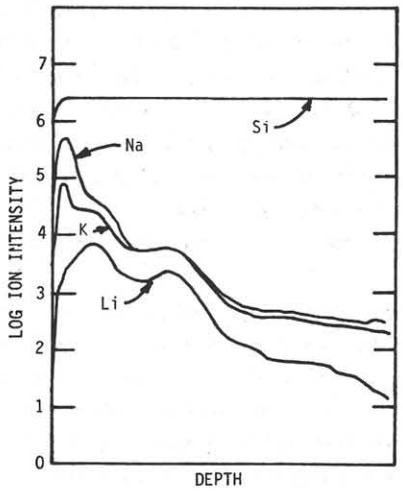

FIGURE 5. Depth profiles from working device.

although from a specimen which failed accelerated life testing. The K appears to be lower in the failed device but the Li is significantly more intense throughout the interior. Having made this comparative observation, analyses such as imaging or careful thin film profiling could then be used to determine the processing step responsible for this contamination.

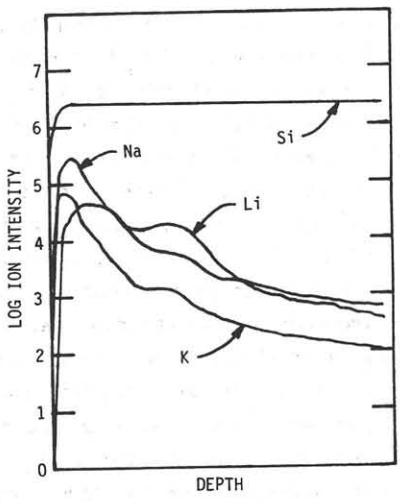

FIGURE 6. Depth profiles from failed device.

Although the devices discussed in Figures 5 and 6 were not available for image analysis, we have extensively studied ionic contamination failure using secondary ion imaging and photographic recording as well as digital image processing. The real power of the imaging mode of operation results from the fact that the ion beam can be moved about on the sample surface to examine different devices, different metallizations or different processing steps. One can also observe these images versus time and get an idea of the three-dimensional distribution of the ionic or any other species present within the devices.

In summary, the SIMS technique is a very powerful method for examining the ionic contaminants contained within a semiconductor device. The ability to image as well as determine in-depth distributions of these ionic species can provide an understanding of the failure mechanism and the incorporation mechanisms for ionic contaminants. It should be noted here that the sensitivity and capabilities of the SIMS technique are not limited solely to the ionic contaminants. One can also use the technique to examine residual photoresist, interfacial vacuum contaminants such as oxygen, carbon, etc., or other foreign substances which may be detrimental to device performance.

IV. Substrate Temperature and Post-Implant Annealing of Se^+-Implanted GaAs.

It had long been known that, in order to achieve high electrical activity after annealing of high-dose ion-implanted Se and Te in GaAs, it is necessary to implant while maintaining the substrate at a temperature greater than 100°C. Takai, et. al., have shown that elevated implant temperatures cause implanted Te to rest on substitutional rather than interstitial sites. The effect of these elevated temperatures on resulting impurity profiles, however, had not been investigated due to the lack of a sensitive analysis technique which could measure as-implanted Se or Te concentrations.

We have used secondary ion mass spectrometry (SIMS) to measure as-implanted profiles of Se in Cr-doped, lightly p-type, and heavily n-type substrates as a function of implant temperature and have found that the Se diffusion during ion implantation is greatly enhanced for substrate temperatures higher than 100°C. No effect of substrate doping was observed in these experiments.

The dramatic influence of the substrate temperature during implantation is shown in Figure 7. The profile shows that there is significantly deeper implantation as a result of increasing the substrate temperature only 100° or 150°C above room temperature. To determine if this greater depth of implantation is due to recoil or conventinal thermal diffusion, a sample was implanted with $^{78}Se^+$ while the substrate was at room temperature. A portion of the $^{78}Se^+$ implanted region was then implanted with $^{80}Se^+$ while the entire GaAs substrate was held at 500°C. That conventional thermal diffusion is not the cause of the profile difference is shown in Figure 8. Recoil effects were ruled out when the $^{78}Se^-$ and $^{80}Se^-$ profiles in Region II of Figure 8 were unchanged from those obtained in Region I and Region III, respectively. We were left with no other explanantion than that radiation enhanced diffusion is the cause of the greater depth of implantation in the case of substrates being held at elevated temperatures.

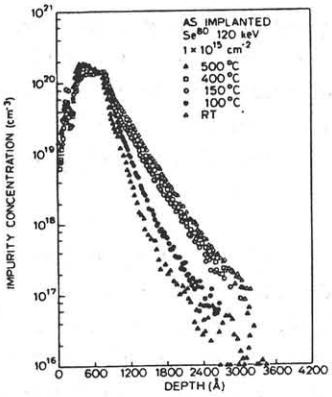

FIGURE 7. SIMS profiles for as-implanted Se at 120 keV to a dose of $1x10^{15}$ atoms/cm^2. Substrate temperatures during implant were 22°C (closed triangles), 100°C (closed circles), 150°C (open circles), 400°C (open squares), and 500°C (open triangles).

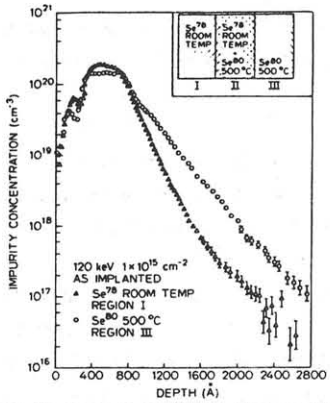

FIGURE 8. As-implanted SIMS profiles for a room temperature implant of Se^{78} at 120 keV to a dose of $1x10^{15}$ atoms/cm^2 (triangles) and the 500°C implant of Se^{80} at 120 keV to a dose of $1x10^{15}$ atoms/cm^2 (circles). In the inset is shown the regions on the substrate for these implants.

Details of these studies are presented in Volume 32 of Applied Physics Letters starting on page 15, page 149 and 572, all during 1978.

V. Direct Analysis of the Rapid Diffusion and Gettering of Oxygen in CZ Silicon

It had been suggested that control of oxygen and carbon in silicon wafers is one of the keys to the successful future of VLSI processing. Oxygen diffusion and precipitation has traditionally been a topic of concern in high temperature silicon processing in relation to swirl, wafer warpage and gettering. However, little information has been available on the motion of oxygen at trace levels into ion implanted or diffused junctions, metallization interfaces and backside damage gettering zones. Inferences have been drawn from bulk measurements after extended anneals at high temperature, but no direct chemical evidence detailing the motion of oxygen at the microscopic level has previously been reported.

In a recent study, it has been demonstrated that bulk oxygen in silicon is rapidly redistributed and gettered into localized structural damage at annealing temperatures as low as 300°C. To determine if techniques could be developed for improving the efficiency of backside gettering during long-term high temperature silicon processing, the initial phase of this study addressed the influence of annealing temperature on damage stability and oxygen redistribution. SIMS depth profiles were obtained for the oxygen distribution within back surface mechanical damage regions after annealing in argon at temperatures of 600°C and 1000°C for variable times. Annealing at 1000°C produces rapid outdiffusion of oxygen to the back surface, but with little or no accumulation after extended anneals at this temperature. However, annealing at 600°C regulsts in a substantial build up of oxygen at the back surface graded through the damage in-depth distribution. If the 600°C anneal is followed by a 1050°C anneal, the amount of oxygen gettering is dramatically increased. This rapid motion and gettering of oxygen has a profound effect on the stability of back surface damage during high temperature processing. Oxygen diffusing into back surface damage at 600°C forms SiO_x precipitates that essentially immobilize or pin damage at the wafer backside, and subsequent annealing at higher temperatures actually increases the gettering efficiency by creating a secondary zone of defects for trapping impurities. Transmission electron micrographs obtained from a vertical cross section through the backside wafer damage show dislocation line defects are generated

at the edge of the initial damage zone creating a damage gettering region extending deeper into the wafer.

Since the majority of the damage is stabilized during the two stage annealing, gettering will continue to be effective through extended high temperature thermal processing. In contrast, single anneals at temperatures greater than 900°C result in rapid annealing of backside damage (within about 30 min.), thereby precluding the gettering of defects and/or heavy metal impurities later in processing. Hence, the rapid motion and damage stabilizing effect of oxygen in silicon can be used advantageously to increase gettering efficiency with the two stage anneal. The process also provides control of intrinsic gettering by SiO_x precipitation since the motion of oxygen into nucleation sites is largely governed by the strain field created at the back surface by the stabilized damage structure.

The study points out that rapid diffusion and gettering of oxygen can prove to be extremely deleterious in wafer processing. In alsmot any step of fabrication, defects and/or strain fields are introduced, that can influence the localized redistribution of oxygen in the active device region. In an extended series of experiments, it was shown that residual damage associated with ion implantation produces rapid motion of oxygen and subsequent formation of SiO_x precipitates within the implanted junctions at annealing temperatures in the range 400°C to 1000°C. Typical oxygen and boron SIMS depth profiles in boron implanted (50 keV, 10^{15} atoms/cm^2) and annealed silicon wafers will be shown. The samples were annealed at 900°C to 1000°C and subsequently annealed at 600°C. Annealing at temperatures of 900°C or 1000°C produces rapid motion and pile-up of oxygen at the front surface of the wafer. If the high temperature anneal is followed by a 600°C anneal, additional motion and gettering of oxygen into residual damage created by the implant is observed. Transmission electron microscopic analyses show that the oxygen is present in the form of SiO_x precipitates within the implant damage. These precipitation zones appear to be relatively stable during additional high temperature processing, suggesting some possible correlation between many of the reported but currently unexplained problems associated with secondary defect nucleation, device shorts, high leakage currents and excessive noise in fabricated devices.

Because of the vulnerability of VLSI devices to microscopic defects, this discovery of the rapid diffusion, gettering and precipitation of oxygen in silicon appears to have an impact on current technology but perhaps more importantly on future submicron device processing requirements. However, additional studies will be necessary to fully assess the correlation of these problems with the observed oxygen behavior in silicon and ultimately, how oxygen motion may be controlled and even advantageously utilized.

The following bibliography gives some references to our use of SIMS and some review papers which intercompare the various surface analytical techniques.

I. General Introduction to SIMS and Studies of Metals and Metal Oxide Systems

"Secondary Ion Mass Analysis: A Technique for Three-Dimensional Characterization," C. A. Evans, Jr., Analytical Chemistry 44, 67A (1971). (Invited article.)

"Analysis of Thin Films by Ion Microprobe Mass Spectrometry," C. A. Evans, Jr., Analytical Chemistry 42, 1060 (1970).

"Ion Microprobe Mass Spectrometric Determination of Oxygen in Copper," C. A. Evans, Jr., Analytical Chemistry 42, 1130 (1970).

"Impurity Distributions in Anodic Films on Tantalum," R. E. Pawel, J. P. Pemsler and C. A. Evans, Jr., Journal of the Electrochemical Society 119, 24 (1972).

"Ion Probe Mass Spectrometry: Overview," C. A. Evans, Jr., Thin Solid Films 19, 11 (1973) and Ion Beam Surface Layer Analysis, J. W. Mayer and J. F. Ziegler, Ed., Elsevier (Lausanne) 1974, p. 11.

(Invited article.)

"Ion Microprobe Analysis for Niobium Hydride in Hydrogen Embrittled Niobium," P. Williams, C. A. Evans, Jr., M. L. Grossbeck and H. K. Birnbaum, Analytical Chemistry 48, 964 (1976).

II. Applications of SIMS to Semiconductor Materials

"Depth Profile Detection Limit of $3x10^{15}$ atom/cm^3 for As in Si Using Cs^+ Bombardment Negative SIMS," C. A. Evans, Jr., and Peter Williams, Applied Physics Letters 30, 559 (1977).

"Evaluation of a Cesium Primary Ion Source on an Ion Microprobe Mass Spectrometer," Peter Williams, R. K. Lewis, C. A. Evans, Jr., and P. R. Hanley, Analytical Chemistry 49, 1399 (1977).

"Anomalous Migration of Fluorine and Electrical Activation of Boron in BF_2-Implanted Silicon," M. Y. Tsai, B. H. Streetman, P. Williams, and C. A. Evans, Jr., Applied Physics Letters 32, 144 (1978).

"Physical and Electrical Properties of Laser-Annealed Ion-Implanted Silicon," A. Gat, J. F. Gibbons, T. J. Magee, J. Peng, V. R. Deline, P. Williams, and C. A. Evans, Jr., Applied Physics Letters 32, 276 (1978).

"Ion Implanted Selenium Profiles in GaAs as Measured by Secondary Ion Mass Spectrometry," A. Lidow, J. F. Gibbons, V. R. Deline, and C. A. Evans, Jr., Applied Physics Letters 32, 15 (1978).

"Fast Diffusion of Elevated Temperature Ion-Implanted Se in GaAs as Measured by Secondary Ion Mass Spectrometry," A. Lidow, J. F. Gibbons, V. R. Deline, and C. A. Evans, Jr., Applied Physics Letters 32, 149 (1978).

"Solid Solubility of Selenium in GaAs as Measured by Secondary Ion Mass Spectrometry," A. Lidow, J. F. Gibbons, V. R. Deline, and C. A. Evans, Jr., Applied Physics Letters 32, 572 (1978).

"Recrystallization of Implanted Amorphous Silicon Layers: II. Migration of Fluorine in BF_2^+-Implanted Silicon," M. Y. Tsai, D. S. Day, B. G. Streetman, P. Williams, and C. A. Evans, Jr., Journal of Applied Physics (in press).

"Gallium Distribution and Electrical Activationof Ga^+-Implanted Si," V. R. Deline, M. Y. Tsai, B. G. Streetman, and C. A. Evans, Jr., Journal of Electronic Materials 8, 111 (1979).

"Use of a Scanning cw Kr Laser to Obtain Diffusion-Free Annealing of B-Implanted Silicon," A. Gat, J. F. Gibbons, T. J. Magee, J. Peng, P. Williams, V. R. Deline and C. A. Evans, Jr., Applied Physics Letters 33, 389 (1978).

"Amorphous-Crystalline Transition of Arsenic Implanted Silicon Caused by Multiple-Pulsed Ruby Laser," J. F. Gibbons, J. L. Regolini, A. Lietoila, T. W. Sigmon, T. J. Magee, J. Peng, J. D. Hong, W. Katz, and C. A. Evans, Jr., Applied Physics Letters, (submitted to).

III. Comparison and Use of Surface Analytical Techniques

"Comparison of Backscattering Spectrometry and SIMS Analysis of Ta_2O_5 Layers," W. K. Chu, M-A. Nicolet, J. W. Mayer, and C. A. Evans, Jr., Analytical Chemistry 46, 2136 (1974).

"Thin Film Compositional Analysis-A Comparison of Techniques," C. A. Evans, Jr., Journal of Vacuum Science and Technology 2, 144 (1975). (Invited article.)

"Effect of Oxidizing Ambients on Platinum Silicide Formation: II Auger and Backscattering Analyses," R. J. Blattner and C. A. Evans, Jr., S. S. Lau, J. W. Mayer, and B. M. Ullrich, Journal of the Electrochemical Society 122, 1732 (1975).

"Interaction of Al Layers with Polycrystalline Si," R. J. Blattner and C. A. Evans, Jr., K. Nakamura, J. W. Mayer and M-A. Nicolet, Journal of Applied Physics 46, 4678 (1975).

"Surface and Thin Film Analysis," C. A. Evans, Jr., Analytical Chemistry 47, 855A (1975). (Invited article.)

"Surface and Thin Film Compositional Analysis: Description and Comparison of Techniques," C. A. Evans, Jr., Analytical Chemistry 47, 818A (1975). (Invited article.) These two invited articles are also being reprinted.

"A Comparison of the Techniques for Silicon Surface Analysis," C. A. Evans, Jr., NBS Workshop Report on the ARPA/NBS Workshop on Surface Analysis for Silicon Devices (NBS, Washington, D.C., 1975), NBS Special Publication SP-400-23.

"Antimony Doping of Si Layers Grown by Solid Phase Epitaxy," S. S. Lau, C. Canali, Z. L. Liau, K. Nakamura, M-A. Nicolet, J. W. Mayer, R. J. Blattner, and C. A. Evans, Jr., Applied Physics Letters 28, 148 (1976).

"Solid-Phase Crystallization of Si Films in Contact with Al Layers," J. Harris, R. Blattner, I. D. Ward, C. A. Evans, Jr., H. L. Fraser, M. Nicolet, and C. L. Ramiller, Journal of Applied Physics 48, 2897 (1977).

Pt_2Si and PtSi Formation with High-Purity Pt Thin-Films," C. Canali, C. Catellani, M. Prudenziati, C. A. Evans, Jr., and W. H. Wadlin, Applied Physics Letters 31, 43 (1977).

"Study of Encapsulants for Annealing of GaAs," K. V. Vaidyanathan, M. J. Helix, D. J. Wolford, B. G. Streetman, R. J. Blattner, and C. A. Evans, Jr., Journal of the Electrochemical Society 124, No. 5 (1977).

"Kinetic Aspects of Solid-Phase Epitaxial Growth of Amorphous Si," Z. L. Liau, S. S. Sau, M. A. Nicolet, J. W. Mayer, R. J. Blattner, P. Williams, and C. A. Evans, Jr., Nuclear Instruments and Methods 149, 623 (1978).

"Profiling Hydrogen in Materials Using Ion Beams," J. F. Ziegler, C. P. Wu, P. Williams, C. W. White, B. Terreault, B. M. U. Scherzer, R. L. Schulte, E. U. Schneid, C. W. Magee, E. Ligeon, J. L'Ecuter, W. A. Lanford, F. J. Kuehne, E. A. Kamukowski, W. O. Hofer, A. Guivarc'h, C. H. Filleux, V. R. Deline, T. Congedo, B. L. Cohen, G. J. Clark, W. K. Chu, C. Brassard, R. S. Blewer, B. R. Appleton, and D. D. Allred, Nuclear Instruments and Methods 149, 19 (1978).

"Modern Experimental Methods for Surface and Thin Film Chemical Analysis," C. A. Evans, Jr., and R. J. Blattner, Surface and Thin Film Chemical Analysis, Annual Review of Materials Science, R. A. Huggins, Ed., Vol. 8 (1978).

"Study of Surface Contaminatin Produced During High-Dose Ion Implantation," M. Y. Tsai, B. G. Streetman, R. J. Blattner and C. A. Evans, Jr., Journal of the Electrochemical Society, 126, 98 (1979).

"Modern Ion Beam and Related Techniques for Materials Characterization," R. J. Blattner and C. A. Evans, Jr., Fifth International Conference on Crystal Growth, Boston, July 17-22, 1977, Proceedings.

"Improved Depth Resolution in Auger Depth Profiling of Multilayered Thin Films by Reactive Ion Sputtering," R. J. Blattner, S. Nadel, and C. A. Evans, Jr., Surface and Interface Analysis, (submitted to).